Supporting Information

Insights into host-guest binding in hydroquinone clathrates: Single-crystal X-ray and neutron diffraction, and complementary computational studies on the hydroquinone-CO_2 clathrate

Arnaud Grosjean,† Peter R. Spackman,† Alison J. Edwards,‡ Kasper Tolborg,¶ Emilie S. Vosegaard,¶ George A. Koutsantonis,*,† Bo B. Iversen,¶ and Mark A. Spackman*,†

† School of Molecular Sciences, University of Western Australia, 35 Stirling Highway, Perth, WA 6009, Australia

‡ Australian Centre for Neutron Scattering, Australian Nuclear Science and Technology Organization, New Illawarra Road, Lucas Heights, New South Wales 2234, Australia

¶ Department of Chemistry and iNANO, Aarhus University, Langelandsgade 140, DK-8000 Aarhus C, Denmark.

Corresponding Author

*Mark Spackman (mark.spackman@uwa.edu.au)

Table of Contents

Section S1. Organic single-crystal structures containing included CO_2

Section S2. Single crystal X-ray and neutron diffraction experiments

Section S3. Summary of crystal structure determinations at 100 K for guest-occupied HQ and β-HQ

Section S4. The CO_2 occupancy in the HQ-CO_2 clathrate

Section S5. Charge density modelling of X-ray and theoretical structure factors for HQ-CO_2

Section S6. Theoretical calculations

Section S7. Supporting references

Tables

Table S1: Crystallographic details and refinement results for X-ray and neutron diffraction data for HQ-CO_2, and X-ray diffraction data for the apohost β-HQ

Table S2: Crystal structure determinations at 100 K for guest-occupied β-HQ compared with the apohost structure

Table S3: Multipole refinement results for 100 K X-ray diffraction data for HQ-CO_2

Table S4: Correlations greater than 0.80 for the multipole refinements in Table S3

Table S5. Multipole refinement results for the set of theoretical structure factors for HQ-CO_2

Table S6: S-HF-3c cell dimensions, elastic tensors and derived properties for β-HQ and HQ-CO_2

Figures

Figure S1: Residual electron density isosurface maps, $\Delta\rho_{residual}$, for the MM-N-1 model

Figure S2: Fractal dimension plots for the MM-N-1 model

Figure S3. Numbering of atoms in HQ-CO_2
Figure S4. Fractal dimension plots for multipole refinements MM-N-0 to MM-N-5
Figure S5. Normal probability plots for multipole refinements MM-N-0 to MM-N-5
Figure S6. CO_2 static model deformation density plots for multipole refinements MM-N-0 to MM-N-5
Figure S7. HQ static model deformation density plots for multipole refinements MM-N-0 to MM-N-5
Figure S8. Static electrostatic potential maps for HQ and CO_2 molecules from the MM-N-2 model.
Figure S9: S-HF-3c Young's modulus in three orthogonal planes for β-HQ and HQ-CO_2
Figure S10: S-HF-3c linear compressibility in three orthogonal planes for β-HQ and HQ-CO_2

S1. Organic single-crystal structures containing included CO_2

The search was based on CSD 5.42 November 2020, with criteria: no errors; not polymeric; no ions; only single crystal structures; only organics; excluding clathrate hydrates and solid CO_2.

'host' molecule	CSD refcode and reference	T / K	year	comments
N,N',N'',N'''-tetramethyl-2,11,20,29-tetra-aza(3.3.3.3)paracyclophane	DERFOV[1]	RT	1984	CO_2 ordered on 2-fold axis with essentially full occupancy. H atoms not located
decamethylcucurbit(5)uril (MeCuc5)	LOZNIX[2]	93	2002	Dodecahydrate; ordered structure with CO_2 in cavity, occupancy 0.76.
4-(3-fluoro-4-trifluoromethylphenyl)-1,2,3,5-dithiadiazolyl	UMASAC[3]	180	2003	CO_2 distributed through channels and not located; CO_2 electron density modelled with SQUEEZE/PLATON
5,11,17,23-tetra-*t*-butyl-25,26,27,28-tetrahydroxycalix(4)arene (*t*BC)	MOVMAM[4] MOVMEQ[4]	RT 125	2008	Two distinct inclusion compounds of *t*BC with CO_2. CO_2 molecules disordered and one of the *t*-butyl groups disordered over two sites
2,4,6,8,10,12-hexanitro-2,4,6,8,10,12-hexaazaisowurtzitane (CL-20)	OLADAH[5] OLADAH01[6] OLADAH02[7]	153 RT 100	2010 2019 2020	Ordered cocrystal structure; explosive
cucurbit[6]uril	UPICOM[8]	90	2010	Synchrotron data; highly disordered, three CO_2 sites, 2 guests in cavity. Highly selective for CO_2 *vs* CO and CH_4. Enthalpy of adsorption is –33 kJ/mol
5,11,17,23-tetra-*t*-butyl-25,26,27,28-tetramethoxy-2,8,14,20-tetra-azacalix(4)arene	FARQUM[9]	133	2012	Highly selective CO_2 uptake. One *t*-butyl group is disordered and CO_2 is bent (165°)
penicilliumine	NOJXIV[10]	100	2014	No atomic coordinates published
4-phenoxyphenol	QIRKUZ[11] QIRLAG QIRLEK	100	2014	Different CO_2 loadings; QIRLEK was crystallized from supercritical CO_2 = 100% occupancy in cavities. CO_2 is trapped in cavities "no strong intermolecular interactions"
1,3,5-tris(4-carboxyphenyl)benzene	PORFIN[12] PORFIN01	323 323	2014 2015	A cocrystal that also incorporates N,N-dimethylformamide. CO_2 molecule disordered over three configurations with occupancy 1/3.
2,8,14,20-tetraethyl-5,11,17,25-tetramethyl-4,24:6,10:12,16:18,22-O,O'-tetra(dimethylsilylene) calix[4]resorcinarene	DABXEM[13]	100	2015	Molecular cavitand; adsorbs many small molecule gases
hydroquinone	ISIVIR[14] ISIVIR01 ISIVIR02	233 100 173	2016	Ordered structures with three different CO_2 occupancies (in order 0.84, 0.72, 0.87)
5,11,17,23-tetramethyl 4,24:6,10:12,16:18,22-O,O'-tetrakis(dimethylsilylene) calix[4]resorcinarene	ILUKAD[15] ILUKIL	100 100	2016	Molecular cavitand with two different CO_2 loadings. Adsorbs many small molecule gases
4,4',4'',4'''-methanetetrayltetrabenzoic acid (adamantanetetrabenzoic acid)	RIJHEA[16]	220	2018	Flexible porous molecular material responsive to CO_2, CH_4 and Xe stimuli. CO_2 molecules disordered over two sites. Synchrotron radiation
4,4'-[(3,3,4,4,5,5-hexafluorocyclopent-1-ene-1,2-diyl)bis(5-methylthiene-4,2-diyl)]dipyridine 1,2,4,5-tetrafluoro-3,6-diiodobenzene	SIKLUW[17]	RT	2018	Porous halogen-bonded framework CO_2 molecules disordered and not modelled; SQUEEZE/PLATON used to model the electron density associated with the included CO_2 molecules
hydroquinone	QOLXAT[18]	137	2019	HQ clathrate with different CO_2:CH_4

	QOLXEX QOLXEX01 QOLXIB QOLXOH QOLYAU QOLYEY QOLYIC	100 100 100 100 100 100 100		ratios of included gases. No coordinates for guest molecules other than CO_2.
10-fluoro-2,3,13a,13b-tetrahydro-1H,8H-pyrrolo[2',1':3,4]pyrazino[2,1-b][1,3]benzothiazine-5,8(6H)-dione	YOZHON[19]	RT	2019	Seems to be ordered cocrystal, but not clear why or how CO_2 is incorporated in this structure.

S2. Single-crystal X-ray and neutron diffraction experiments

Synthesis and crystallization

Crystals of HQ-CO_2 were prepared by a modification of the literature procedure.[14] A stainless steel autoclave (Carl-Roth, 120 mL) containing a glass liner was charged with α-HQ (5.2 g, 0.047 mol) in ethanol (12.5 mL), the autoclave flushed by two successive charges of CO_2 and finally charged with 20 bar (2.0 MPa) of gas. The reaction was left at ambient temperature for 16 hrs without stirring. The autoclave was depressurised slowly and the crystals collected by vacuum filtration.
Crystals of the β-HQ apohost were prepared by dissolving 0.5521 g α-HQ in 10 mL propan-2-ol, and allowing the solvent to evaporate for one week in a fume hood at room temperature. Large single crystals (>1 mm) that formed were cut to obtain reasonably sized crystals for X-ray diffraction experiments.

Single-crystal X-ray diffraction

X-ray diffraction data for HQ-CO_2 were measured on an Oxford Diffraction Xcalibur diffractometer equipped with a Sapphire3 CCD detector using graphite monochromated Mo-Kα radiation generated from a sealed tube (0.71073 Å). Crystals were kept at 100 K using an Oxford Instruments CryojetXL™ nitrogen gas-stream cooling device. The scan width was chosen to be 1° per frame and the crystal to detector distance was fixed at 50 mm. Data integration and reduction were carried out using CrysAlis Pro.[20] Using the Olex2 interface[21] the crystal structure was first solved and refined using SHELXTL.[22] Data merging was performed using SORTAV within the WinGX package.[23]
The β-HQ crystal was mounted on a goniometer with paratone-N oil, and kept at 100 K using the liquid nitrogen stream in an Oxford Cryosystems Cryostream 700 device. X-ray diffraction data were collected on an Agilent Technologies SuperNova diffractometer fitted with a microfocus Mo Kα source. Data were collected using ω-scans with a scan width of 1° and an exposure time of 70 s per frame. The crystal to detector distance was fixed at 52 mm. Data integration, structure solution and refinement were carried out as for HQ-CO_2.

Single-crystal Laue neutron diffraction

A high quality elongated square prismatic crystal approximately 1.5 x 1.5 x 2.5 mm was mounted to the ϕ axis of the KOALA diffractometer standing at the end of the TG3 supermirror guide at the OPAL nuclear reactor, ANSTO. The crystal was cooled in the open flow of an Oxford Cryosystems COBRA™ 100 K nitrogen stream. Two sets each of 19 images were collected from the stationary crystal with 17° ϕ rotation between frames. Owing to the size of the crystal, two sets of exposures, one at 600 s and one at 1500 s allowed extraction of an optimal data set with the strongest reflections well measured on the short exposure frames and the less intense reflections better measured on the longer exposures. Data reduction by means of the LaueG[24] suite incorporating ArgonneBoxes[25] was extended to a relatively high resolution with all uniquely indexable reciprocal lattice points to a d-spacing of 0.65 Å for all wavelengths $0.85 \leq \lambda < 1.7$Å included in the integration and normalization. The overall R_{int} for all data extracted in this manner is as is typical for such experiments meaningless due to the large number of very weak data and the inherently high background in the experiment whereas R_{int} for the 4σ data 0.081(47) demonstrates that the merging of all data across the different exposures is appropriate. Structure refinement[26] commenced from the X-ray model coordinates and after scale factor refinement only, a difference map phased on the non-hydrogen atom positions revealed all of the hydrogen atom sites to be fully ordered. A full-matrix least-squares refinement on F of all atomic sites modelled with anisotropic displacement parameters, together with a common occupancy for the C and O sites of the CO_2 and subject to a suitable weighting scheme converged to R = 4.57%, R_w = 4.40% and S = 1.47 for 70 parameters and 659 observsations $I \geq 3\,\sigma I$. At convergence, the CO_2 occupancy was 0.856(17) and the difference density maps were featureless at +/- ~0.63 fm Å^3 well below the value corresponding to any atom of this structure. It is notable that the data set extracted from the two different exposure length frames yields sufficient observations to approach 10 independent observations per refined parameter.

Crystallographic details, spherical atom refinement of X-ray and neutron diffraction data are summarized in **Table S1**.

Table S1. Crystallographic details and refinement results for 100 K X-ray and neutron diffraction data for HQ-CO_2, and X-ray diffraction data for the apohost β-HQ.

Chemical formula	$3C_6H_6O_2.xCO_2$		$C_6H_6O_2$
Crystal system, space group	trigonal, $R\bar{3}$		trigonal, $R\bar{3}$
a, c (Å)	16.1737(2), 5.7050(10)		16.5721(12), 5.3599(4)
V (Å^3)	1292.42(3)		1274.8(2)
Z	9		9
Data collection	**X-ray**	**Neutron**	**X-ray**
T (K)	100.4(8)	100.0(1)	100.0(1)
Wavelength (Å)	0.71073	$0.85 < \lambda < 1.7$	0.71073
Crystal size (mm^3)	0.18 × 0.22 × 0.33	1.5 × 2.5 × 2.5	0.3 × 0.2 × 0.1
Completeness	99.8%	84.1%	99.9%
$N_{measured}$, N_{unique}	39813, 2817	23079, 921	2565, 831
R_{int} [a]	2.54 %	8.1 (4.7) %	3.32 %
$(\sin\theta/\lambda)_{max}$ (Å^{-1})	1.12	1.11	0.72
Independent atom model refinement	**X-ray**	**Neutron**	**X-ray**
Refinement on	F^2 (for $F > 4\sigma(F)$)	F (for $I > 3\sigma(I)$)	F^2 (for $F > 4\sigma(F)$)
R, wR, S [b]	3.92, 11.53, 1.146	4.57, 4.40, 1.471	3.90, 10.40, 1.070
N, P	3389, 55	659, 70	763, 41
x (fractional CO_2 occupancy)	0.882(5)	0.856(17)	na
Deepest hole/highest peak in the residual Fourier map	–0.17, 0.77 e Å^{-3}	–0.67, 0.60 fm Å^{-3}	–0.21, 0.68 e Å^{-3}

[a] $R_{int} = \sum\left|F^2_{obs} - \langle F^2_{obs}\rangle\right| / \sum F^2_{obs}$. For the neutron data R_{int} refers to the merge of normalized multiple wavelength data for 6964 reflections with $I > 4\sigma(I)$.ref??

[b] $R(F^2) = 100\sum|F^2_{obs}| - |F^2_{calc}| / \sum|F^2_{obs}|$, $wR(F^2) = 100\sqrt{\sum w(F^2_{obs} - F^2_{calc})^2 / \sum w(F^2_{obs})^2}$,

$S = \sqrt{\sum w(F^2_{obs} - F^2_{calc})^2 / (N - P)}$ with $w = 1/\sigma^2_{obs}$, N the number of reflections and P the number of independent parameters

S3. Summary of single-crystal structure determinations at 100 K for empty and guest-occupied β-HQ.

Table S2. Crystal structure determinations at 100 K for guest-occupied β-HQ compared with the apohost structure. *a* and *c* are the two cell lengths in the trigonal cell, and the occupation numbers refer to fractional occupation of the cavity. $d_{O\cdots O}$ is the distance between oxygen atoms in the six-membered hydrogen-bonded ring, and θ is the angle between the HQ phenyl ring plane and the *ab* plane of the unit cell.[a]

CSD refcode	*a*	*c*	*V* / Å^3	$d_{O\cdots O}$ / Å	θ / °	Guest (occupation)
β-HQ [b]	16.5721(12)	5.3599(4)	1274.8	2.659	55.2	-
JAMKEN02 [27]	16.580(4)	5.424(2)	1291.3	2.682	55.5	Xe
QOLXEX [18]	16.4158(10)	5.4958(3)	1282.6	2.672	56.8	CO_2 (0.71) [c]
ZZZVLI02 [28]	16.4604(4)	5.5047 (2)	1291.7	2.686	56.6	CH_3OH
QOLXEX01[18]	16.3515(9)	5.5688(4)	1289.5	2.677	57.6	CO_2 (0.73) [c]
QOLXOH [18]	16.3254(4)	5.5730(2)	1286.3	2.675	57.7	CO_2 (0.59) / CH_4 (0.23) [d]
QOLXIB [18]	16.3211(6)	5.5798(2)	1287.2	2.675	57.8	CO_2 (0.58) / CH_4 (0.23) [d]
QOLYAU [18]	16.265(2)	5.623(8)	1288.3	2.675	58.3	CO_2 (0.71) / CH_4 (0.16) [d]
QOLYEY [18]	16.2353(8)	5.6439(3)	1288.3	2.676	58.6	CO_2 (0.75) / CH_4 (0.08) [d]
QOLYIC [18]	16.1884(6)	5.6876(3)	1290.8	2.678	59.1	CO_2 (0.83) [d]
ISIVIR01 [14]	16.2023(11)	5.6943(4)	1294.6	2.680	59.1	CO_2 (0.87)
HQ-CO_2 [b]	16.1737(2)	5.7050(10)	1292.4	2.679	59.2	CO_2 (0.90)
HQUACN02 [28]	15.8352(4)	6.1919(2)	1344.6	2.736	63.2	CH_3CN

[a] θ is not the same as the angle α of the rhombohedral unit cell, but the two are in fact strongly correlated (R^2 = 0.979 for the structures in the table)

[b] Present work (see Table S1)

[c] These structures were refined with different occupancies for the atoms of the CO_2; the occupancy reported here is for the carbon atom.

[d] These gas occupancies have an estimated uncertainty of ±0.06.[18]

S4. The CO_2 occupancy in the HQ-CO_2 clathrate

Previous work

There is disagreement in the literature regarding the occupancy of CO_2 in the HQ-CO_2 clathrate, but this needs to be considered in the context of the different preparation methods, as well as the different analytical approaches used to obtain this quantity. In the original report by Palin & Powell[29] solid carbon dioxide CO_2 was added to an aqueous saturated solution of HQ in a Parr bomb, which was heated to 50° and then cooled slowly to room temperature. Chemical analysis yielded 8.9 wt%, $x = 0.74$. The same value was obtained from the X-ray cell dimensions, but no detail was provided. A decade later Peyronel & Barbieri[30] described synthesis using a saturated solution of HQ in ethanol in a stainless steel bomb at 35°; after flushing air the bomb was filled with CO_2 gas and the solution was cooled over eight hours. The pressure inside the bomb was kept constant during the cooling period. The maximum value found was $x \sim 0.75$, and this was reported to *decrease* at pressures above ~20 atm (2 MPa). A similar synthetic approach was used by McAdie.[31] Initial $p(CO_2)$ was 700 psi (4.8 MPa) and the fraction of clathrate cavities occupied by guest molecules was determined by dissolving known mass of clathrate in ethanol and drying to constant weight at 40°C. Analysis gave $x = 0.75$.

In a series of studies by Yoon and co-workers HQ clathrates of small gas molecules were prepared by a solid-gas reaction, charging powdered HQ in a high-pressure cell and allowing it to react with pure gases or gas mixtures. After loading the HQ the cell was purged and pressurized. For studies with mixed CO_2/N_2 gases at 20, 40, 60 and 80 mol% CO_2, and 1.0, 2.0 and 3.0 MPa total gas pressure, the maximum $x = 0.91$ was found with 80 mol% CO_2 and 3.0 MPa.[32] In separate work HQ-CO_2 was synthesized using $p(CO_2) = 4$ MPa for 30 h. The crystalline product was determined by X-ray diffraction to have a hexagonal unit cell of $a = 16.29$ Å and $c = 5.81$ Å and elemental analysis showed that x is approximately 0.74.[33] A later study with mixed CO_2/N_2 gases used gas mixtures with 20, 40, 60 and 80 mol% CO_2, and total pressures of 10, 20, 30 and 50 bar (1.0, 2.0, 3.0 and 5.0 MPa). Elemental analysis gave x just under 1.0 for 5.0 MPa and pure CO_2, but x was found to be less for lower pressures used in synthesis. Spectroscopic and elemental analyses suggested that the CO_2 occupancy is enhanced as the synthesis pressure increases, or as the CO_2 concentration in the feed gas increases. Quantitative analyses (^{13}C solid-state NMR and elemental) showed that at larger CO_2 partial pressures x increases to 0.90.[34] In the most recent report from Yoon *et al.*,[35] clathrates of HQ with CH_4 and with CO_2 were prepared using pure gases and gas pressures of 3.0 and 5.0 MPa. NMR and elemental analysis yielded for HQ-CO_2 $x = 0.901(39)$ for 3.0 MPa and 0.994(27) for 5.0 MPa gas pressures.

For their crystal structure determination of HQ-CO_2 Torré, Coupan *et al.* described[14] synthesis from a solution of HQ in ethanol, with CO_2 pressure ramped up to 20 bar (2.0 MPa). TGA/MS analysis gave CO_2 stored 8.9 wt%, corresponding to occupancy $x = 0.71$. Their X-ray refinement yielded $x = 0.87$, but the authors commented: "While higher than the value from TGA, this figure is strongly correlated to the thermal ellipsoids. The CO_2 molecule is not really fixed in the cavity, so we could expect an overestimation, and in this particular case crystallography gives only an idea but not an accurate value for this occupancy. By fixing the occupancy of CO_2 to 71% in the structure model, the thermal ellipsoids become nearly perfect in comparison to the host molecule, but the R value increases from 0.0362 (for all data with 87% occupancy) to 0.0442 (for all data with 71% occupancy). Probably the real occupancy lies between these values."

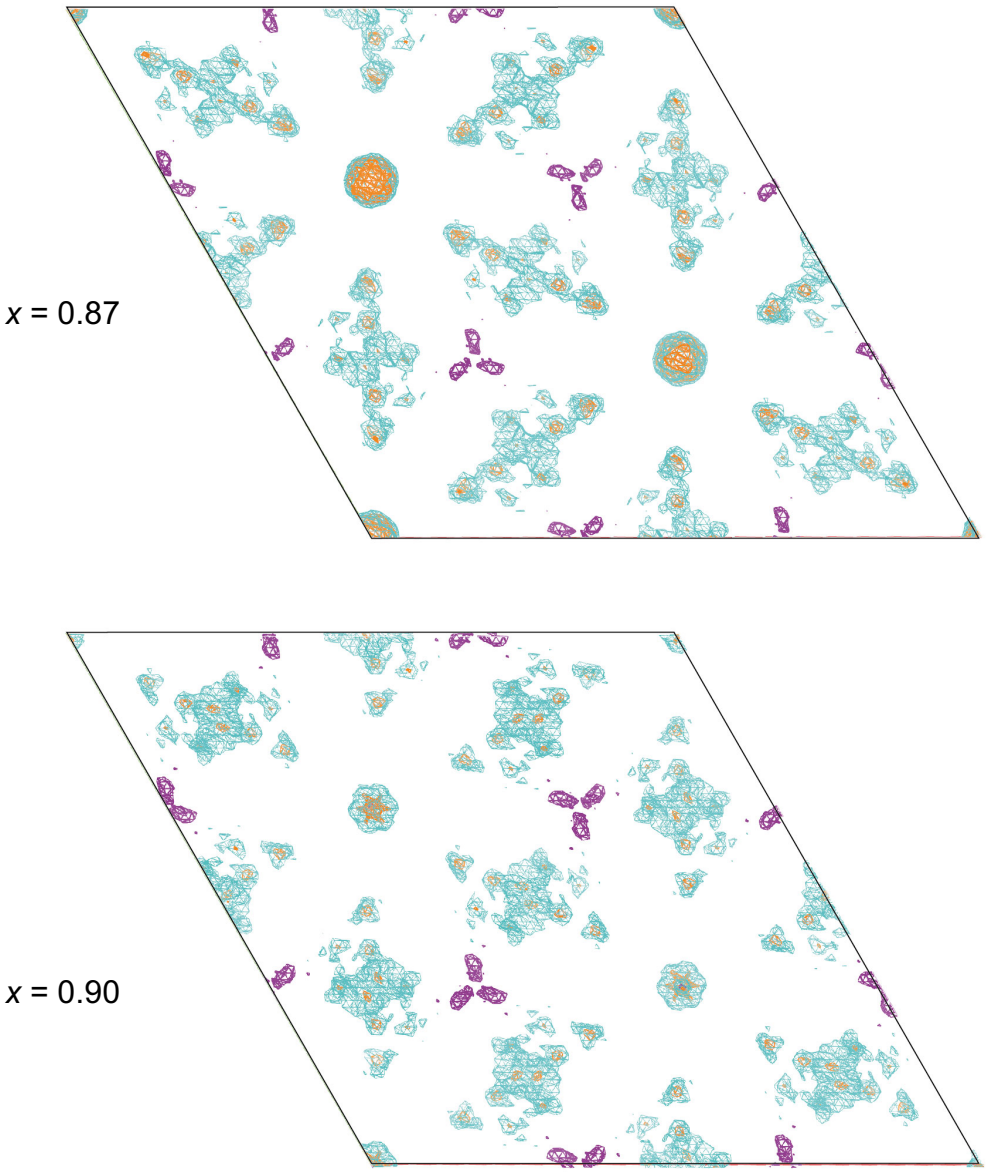

Figure S1. Residual electron density isosurface maps, $\Delta\rho_{residual}$, for MM-N-1 model. Top: CO_2 occupancy of 0.87; extrema are –0.15 and +0.36 e Å^{-3}. Bottom: CO_2 occupancy of 0.90; extrema are –0.14 and +0.21 e Å^{-3}. Isovalues are +0.15 e Å^{-3} (orange), +0.10 e Å^{-3} (cyan) and –0.10 e Å^{-3} (purple).

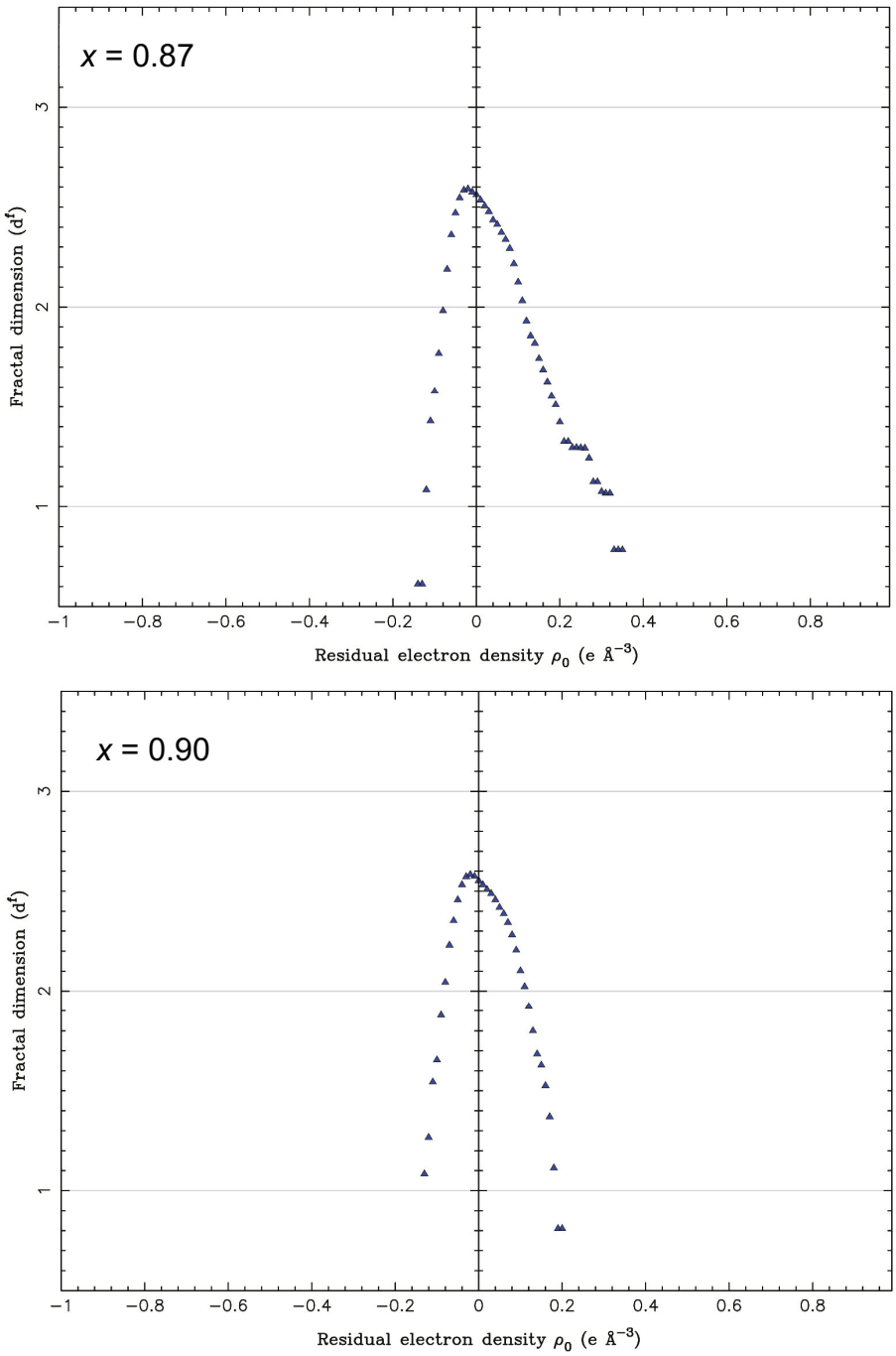

Figure S2. Fractal dimension plots for the MM-N-1 model assuming CO_2 occupancies of 0.87 (top) and 0.90 (bottom).

S5. Charge density modelling of X-ray and theory structure factors for HQ-CO_2

Multipole refinement details

Comparison between X-ray and neutron ADPs[36] for the six heavy atoms in HQ-CO_2 showed a mean ratio of diagonal terms, U_{ii}(X-ray)/ U_{ii}(neutron) = 0.669(50)). The scale factor, atomic positions, and ADPs of non-hydrogen atoms were initially refined against high-angle X-ray data ($\sin\theta/\lambda > 0.80$ Å^{-1}). Hydrogen atom positions and scaled ADPs from the neutron structure refinement were introduced and anharmonic motion of the CO_2 molecule was explored by introducing higher-order Gram-Charlier coefficients into the high-angle refinement (3rd and 4th on O(2), 4th only on C(6)). Only the 3rd-order coefficients on O(2) were found to be significant, resulting in a lowering of $R_w(F^2)$ from 5.39% to 4.65%. The unique coefficients [C_{111} = -0.000047(16), C_{333} = 0.000730(506), C_{112} = -0.000087(16) and C_{113} = -0.001091(35)] were fixed in all subsequent refinements, in addition to the neutron hydrogen atom positions and scaled ADPs.

For the multipole refinements charge neutrality constraints were employed for the molecular fragments, and no local symmetry constraints were imposed on multipole populations on HQ. Core and valence monopole scattering factors were from Stewart's localized orbitals derived from Hartree-Fock wavefunctions,[37] and single exponential functions described the radial part of higher multipoles. The multipole expansion for non-hydrogen atoms extended to hexadecapoles, while that for hydrogen atoms extended to quadrupoles. The electron density model of CO_2 was constrained to have cylindrical symmetry (i.e. they were modelled as cylindrically symmetric so O3+, O3–, H3+ and H3– were not included on O(2) and C(6)), with thermal motion in line with the 3-fold symmetry of its site on the *c*-axis). Six MM-N models were explored, with radial flexibility increasing from κ and κ' fixed to default values (MM-N-0) to all κ and κ' varied (MM-N-5).

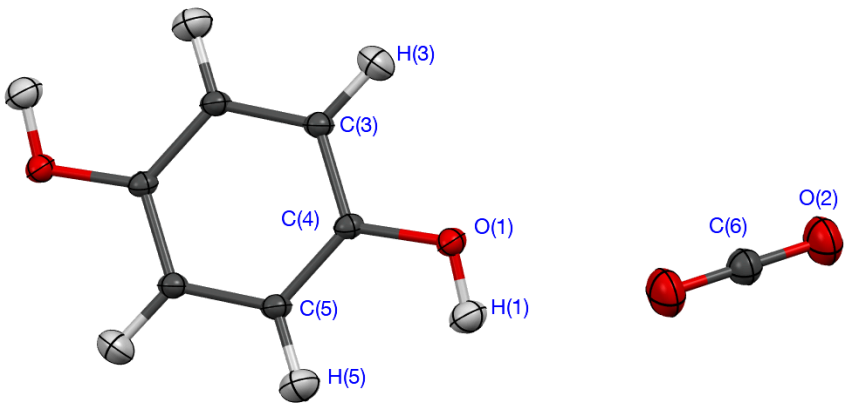

Figure S3. Numbering of atoms in HQ-CO_2. Inversion centres lie at the centre of the phenyl ring and at atom C(6). Ellipsoids from the neutron refinement are displayed at 50% level.

Multipole refinement results – X-ray structure factors

Table S3. Multipole refinement results for 100 K X-ray diffraction data for HQ-CO_2. All refinements based on F^2, with $F^2 > 3\sigma(F^2)$; $w = 1/\sigma(F^2)$; 2817 reflections. The CO_2 occupancy was fixed at 0.90.

Multipole model	**MM-N-0**	**MM-N-1**	**MM-N-2**	**MM-N-3**	**MM-N-4**	**MM-N-5**	**MM-SHADE**
brief description	no kappas refined	+ κ and κ' on O(1), C(3), C(4), C(5)	+ refine κ(H) = κ'(H)	+ refine κ(O(2)) and κ(C(6))	+ refine κ'(O(2)) and κ'(C(6))	constrain κ and κ' by atom type	MM-N-1 model using SHADE3 ADPs
R	4.26	3.48	3.49	3.47	3.38	3.54	3.53
$wR(F^2)$	4.25	3.82	3.81	3.79	3.76	3.79	3.82
S	1.281	1.151	1.150	1.143	1.135	1.143	1.153
P	174	180	181	183	185	187	180
C=O / Å	1.1493	1.1485	1.1485	1.1496	1.1459	1.1488	1.1485
DMSDA / $Å^2$	1	-7	-7	2	8	-1	-7
$\Delta\rho_{max}$ / $eÅ^{-3}$	0.314	0.205	0.211	0.181	0.175	0.184	0.217
$\Delta\rho_{min}$ / $eÅ^{-3}$	-0.141	-0.136	-0.137	-0.139	-0.138	-0.138	-0.139
Θ / DÅ	-3.23(31)	-4.18(29)	-4.23(29)	-5.99(49)	-8.64(52)	-7.68(28)	-4.28(29)
κ(O(1))	1.0	0.979(1)	0.982(1)	0.984(1)	0.983(1)	0.986(1)	0.983(1)
κ'(O(1))	1.0	0.996(16)	0.983(16)	0.971(15)	0.976(15)	1.002(16)	0.978(15)
κ(O(2))	1.0	1.0	1.0	0.996(2)	1.000(3)	as for O(1)	1.0
κ'(O(2))	1.0	1.0	1.0	1.0	1.428(90)	"	1.0
κ(C(3)) = κ(C(5))	1.0	1.032(2)	1.036(2)	1.044(2)	1.043(2)	1.040(2)	1.028(2)
κ'(C(3)) = κ'(C(5))	1.0	0.795(5)	0.797(5)	0.797(5)	0.796(5)	0.827(4)	0.808(5)
κ(C(4))	1.0	1.025(2)	1.027(2)	1.036(3)	1.035(3)	as for C(3)	1.025(2)
κ'(C(4))	1.0	0.884(9)	0.886(10)	0.885(9)	0.880(9)	"	0.879(9)
κ(C(6))	1.0	1.0	1.0	1.068(7)	1.010(7)	"	1.0
κ'(C(6))	1.0	1.0	1.0	1.0	0.717(17)	"	1.0
κ(H) = κ'(H)	1.2	1.2	1.156(10)	1.150(10)	1.160(10)	1.153(9)	1.2

Table S4. Correlations greater than 0.80 for the multipole refinements in Table S3. For each refinement the correlation coefficient is given along with the relevant XD2016 parameters; correlations involving parameters on O(2) and C(6) are in red. Note that the charge neutrality constraint for the CO_2 molecule means that M1(O(2)) and M1(C(6)) are necessarily constrained with a correlation coefficient of 1.00.

MM-N-0	0.82	U33(O(2))···Q0(O(2))				
MM-N-1	0.81	U33(O(2))···Q0(O(2))	0.81	O2-(C(4))···κ'(C(4))		
MM-N-2	0.81	O2-(C(4))···κ'(C(4))	0.81	U33(O(2))···Q0(O(2))	0.87	M1(H(5))···κ(H)
	0.90	M1(H(1))···κ(H)				
MM-N-3	0.81	O2-(C(4))···κ'(C(4))	0.82	z(O(2))···D0(O(2))	0.82	O1-(C(4))···κ'(C(4))
	0.83	U33(O(2))···Q0(O(2))	0.85	M1(C(6))···κ(C(6))	0.86	M1(H(5))···κ(H)
	0.87	M1(H(3))···κ(H)	0.89	M1(H(1))···κ(H)		
MM-N-4	0.81	O2-(C(4))···κ'(C(4))	0.82	O1-(C(4)··· κ'(C(4))	0.83	U33(O(2))···U12(O(2))
	0.83	U11(O(2))···U33(O(2))	0.86	U12(O(2))···Q0(O(2))	0.86	U22(O(2))···Q0(O(2))
	0.87	M1(H(5))···κ(H)	0.88	M1(H(3))···κ(H)	0.90	M1(C(6))···κ(C(6))
	0.90	M1(H(1))···κ(H)	0.93	U33(O(2))···Q0(O(2))		
MM-N-5	0.81	κ(C)···SCALE	0.84	M1(H(5))···κ(H)	0.86	M1(H(3))···κ(H)
	0.88	M1(H(1))···κ(H)				
MM-SHADE	0.81	U33(O(2))···Q0(O(2))	0.82	O1-(C(4))···κ'(C(4))		

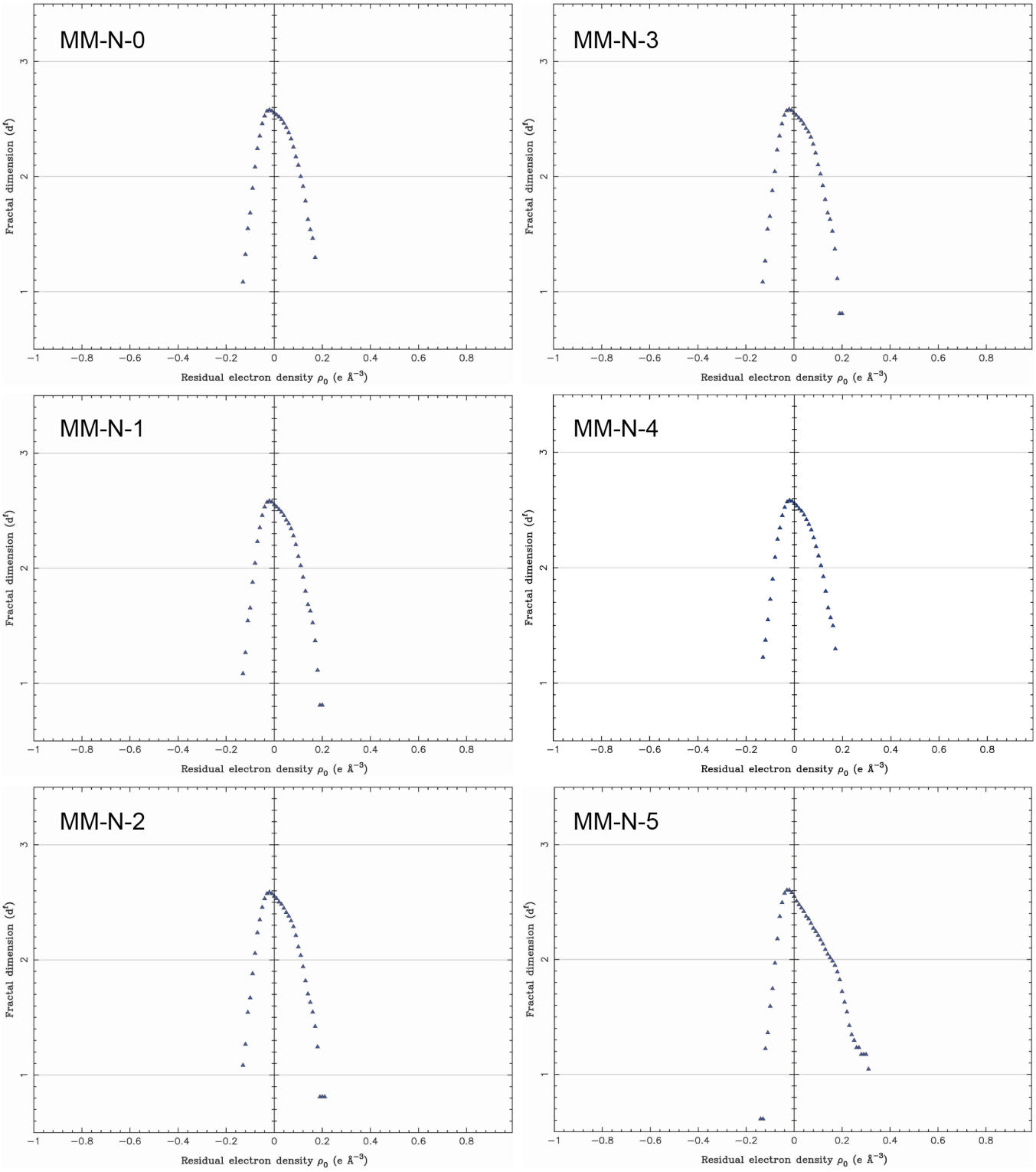

Figure S4. Fractal dimension plots for multipole refinements MM-N-0 to MM-N-5 in Table S3.

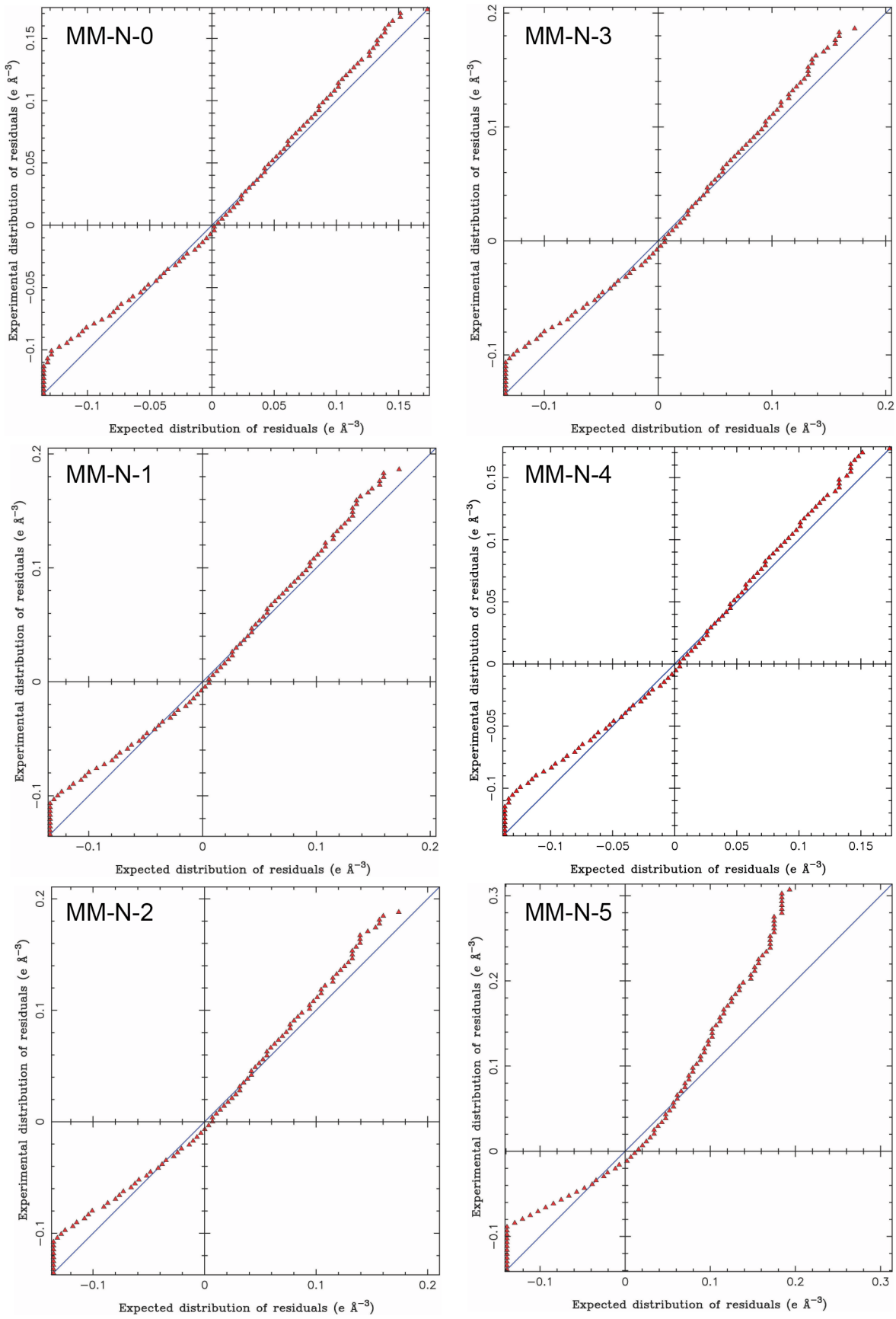

Figure S5. Normal probability plots for the MM-N for multipole refinements MM-N-0 to MM-N-5 in Table S3.

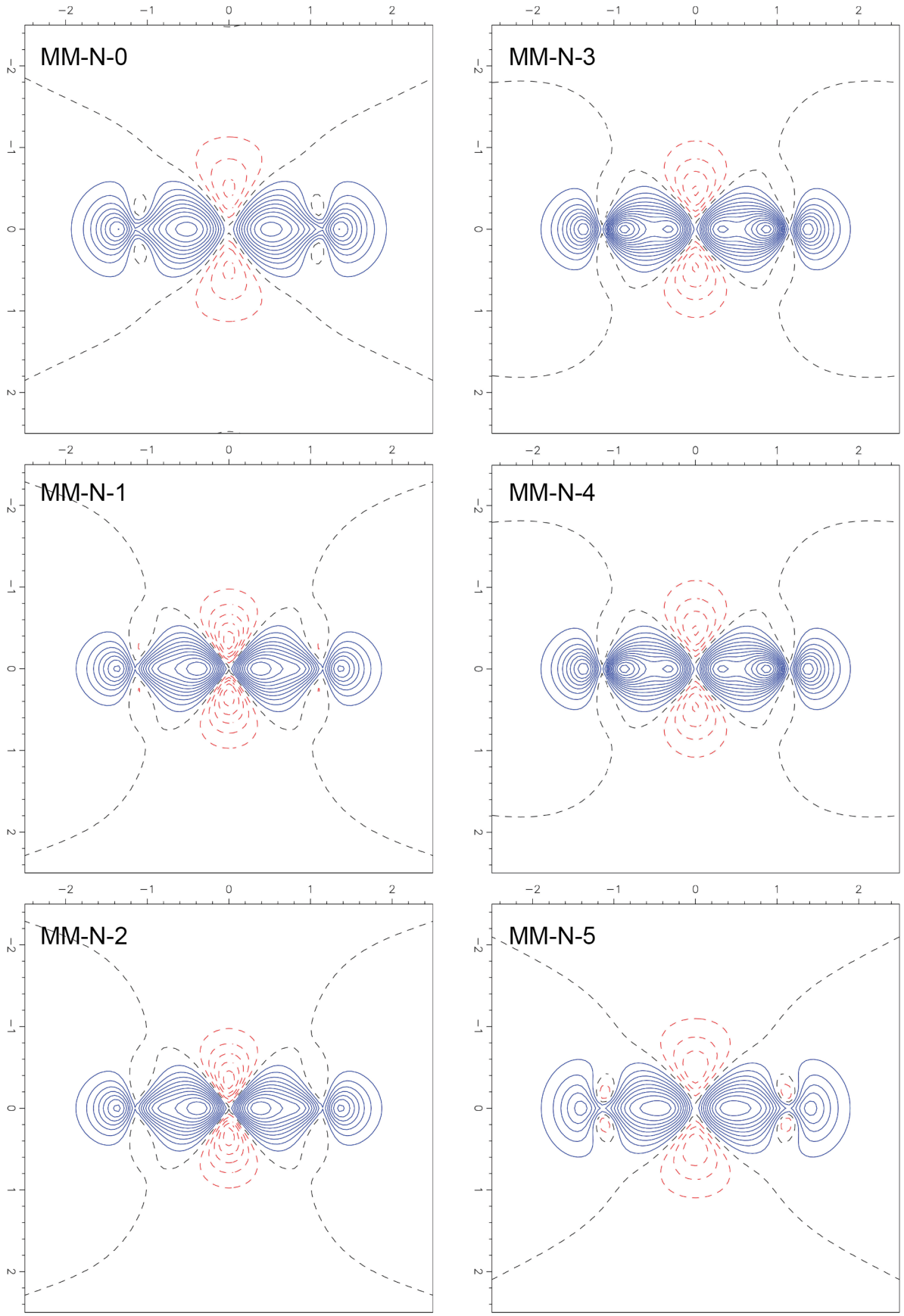

Figure S6. CO_2 static model deformation density plots for multipole refinements MM-N-0 to MM-N-5 in Table S3. Contours are at intervals of 0.1 e Å^{-3}.

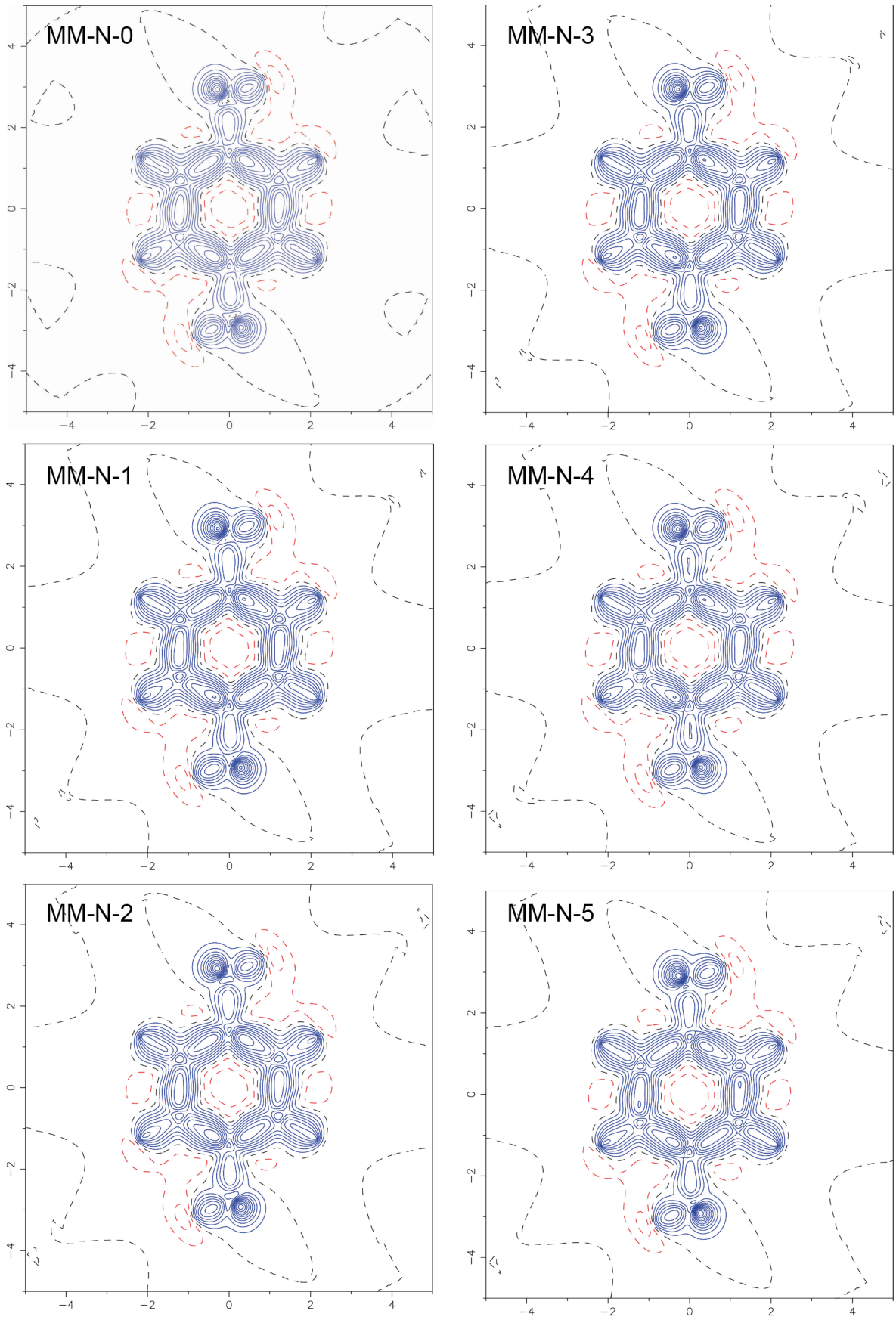

Figure S7. HQ static model deformation density plots for multipole refinements MM-N-0 to MM-N-5 in Table S3. Contours are at intervals of 0.1 e Å^{-3}.

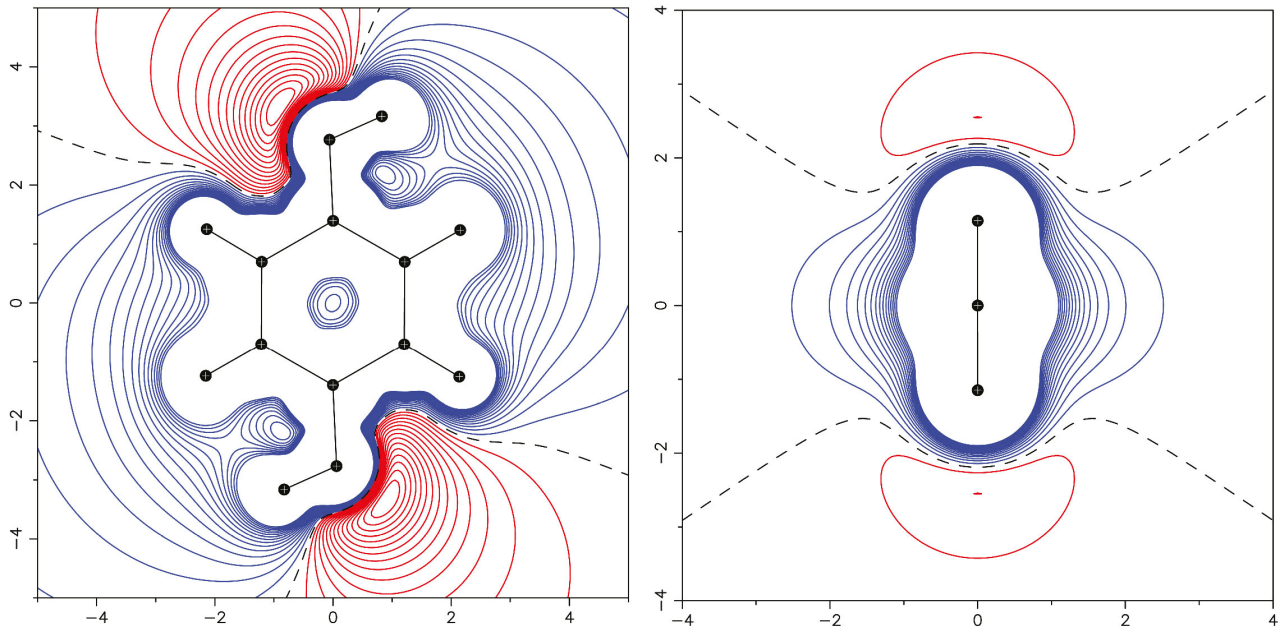

Figure S8. Static electrostatic potential maps for hydroquinone (left; 10 Å square) and CO_2 (right; 8 Å square) molecules from the MM-N-2 model. Mapping planes are the same as in Figures S7 and S8. Contour intervals are 0.025 e $Å^{-1}$, and blue lines are positive and red lines negative.

Multipole refinement results – theoretical structure factors

Table S5. Multipole refinement results for the set of theoretical structure factors for HQ-CO_2. All refinements based on F^2 using the same set of reflections as the X-ray data. The CO_2 occupancy was 1.00 and unit weights were used.

Multipole model	**MM-N-0**	**MM-N-1**	**MM-N-2**	**MM-N-3**	**MM-N-4**	**MM-N-5**
brief description	no kappas refined	+ κ and κ' on O(1), C(3), C(4), C(5)	+ refine κ(H) = κ'(H)	+ refine κ(O(2)) and κ(C(6))	+ refine κ'(O(2)) and κ'(C(6))	constrain κ and κ' by atom type
$R(F^2)$	1.16	1.04	1.04	0.95	0.92	0.99
Θ / D Å	-3.47	-3.77	-3.78	-4.5	-4.62	-4.18
κ(O(1))	1.000	0.990	0.990	0.988	0.989	0.996
κ'(O(1))	1.000	1.136	1.136	1.133	1.129	1.156
κ(O(2))	1.000	1.000	1.000	1.004	1.002	0.996
κ'(O(2))	1.000	1.000	1.000	1.000	1.238	1.156
κ(C(3)) = κ(C(5))	1.000	1.002	1.003	1.002	1.003	1.007
κ'(C(3)) = κ'(C(5))	1.000	0.925	0.928	0.928	0.928	0.921
κ(C(4))	1.000	1.011	1.011	1.009	1.009	1.007
κ'(C(4))	1.000	0.944	0.940	0.933	0.935	0.921
κ(C(6))	1.000	1.000	1.000	1.052	1.035	1.007
κ'(C(6))	1.000	1.000	1.000	1.000	0.868	0.921
κ(H) = κ'(H)	1.200	1.200	1.188	1.185	1.184	1.155

S6. Theoretical calculations

Theoretical structure factors for HQ-CO_2

Theoretical structure factors were obtained with CRYSTAL17[38] using the 100 K geometry of HQ-CO_2 from the neutron diffraction experiment, and the B3LYP functional[39] with the POB-TZVP basis set.[40] Static structure factors corresponding to those measured in the X-ray diffraction experiment were calculated as the Fourier transform of the periodic electron density.

Host-guest interactions

Plane-wave DFT optimisations were performed using the VASP[41]software package, employing the PBE[42] functional and Grimme's D3 dispersion correction[43] with Becke-Johnson damping (GD3BJ).[44] VASP optimizations were performed using a 500 eV energy cut-off for the plane wave basis, with convergence tolerances of 10^{-7} eV per atom in the electronic minimization and 3 x 10^{-2} eV $Å^{-1}$ in the forces for the geometry optimization, and Γ-centered *k*-point grids spaced at a minimum of 0.05 $Å^{-1}$. Final energies were obtained by performing a single-point energy evaluation on the optimized structures using the same functional and dispersion correction, but instead with a tighter convergence criterion and cut-off of 700 eV for the plane-wave basis. All calculations in VASP made use of the projector-augmented wave (PAW) method[45] and the standard supplied pseudopotentials.[46] In order to speed up the optimization procedure, the rhombohedral cell setting (with unit cells 1/3 of the size) for the crystals was used rather than the equivalent hexagonal setting.
CE-B3LYP energies use electron densities of unperturbed monomers to estimate electrostatic, polarization, and repulsion energies, which are combined with Grimme's D2 dispersion corrections, with the four separate energy components scaled to best fit B3LYP-D2/6-31G(d,p) counterpoise-corrected energies for molecule/ion pairs extracted from a large number of crystal structures.[47] CrystalExplorer17 was used to compute CE-B3LYP energies, and Gaussian09[48] for all calculations on isolated molecules (including the monomer wavefunctions in the CE-B3LYP model).

Harmonic vibrational motion

Starting from the previously optimized crystal geometries, these crystals were converted back to their hexagonal setting, then a 1 x 1 x 2 supercell was constructed, with cell lengths of approximately (16 Å, 16 Å and 12 Å), making it sufficiently large to avoid almost all self-image interactions which may lead to negative frequencies. The Phonopy[49] software was used to generate the various displacements in order to calculate the phonons by finite differences of the force-constants, and single point energies and force calculations were performed using the same procedure outlined for the final energy calculations of the host-guest crystals.

Young's modulus and linear compressibilities

Elastic tensors for *β*-HQ and HQ-CO_2 (Table S6) were obtained with CRYSTAL17[38] using the ELASTCON module[50] with default convergence criteria and numerical second derivatives computed from a fit to three points. The S-HF-3c variant of the small basis set corrected Hartree-Fock method HF-3c was used (i.e. a scaling factor of s_8 = 0.7), representing a balance between computational efficiency and the reliable description of crystal structure and cohesive energy for a wide range of organic molecular crystals.[51] We have calibrated the performance of this approach through a detailed comparison between S-HF-3c computed elastic tensors and experimental measurements for 42 molecular crystals, focusing on computed and experimental crystal structures, bulk modulus, anisotropy of the elastic tensor, and extreme values of the Young's modulus and linear compressibility.[52] ELATE[53] was used for the analysis of the elastic tensors and creation of the plots in Figures S10 and S11.

Table S6. S-HF-3c cell dimensions, elastic tensors and derived properties for β-HQ and HQ-CO_2.

		β-HQ	HQ-CO_2
cell dimensions / Å	a	16.818	16.203
	c	4.930	5.462
elements of elastic tensor / GPa	$C_{11} = C_{22}$	30.24	26.23
	C_{12}	18.25	15.56
	$C_{13} = C_{23}$	14.41	14.02
	$C_{14} = -C_{24} = C_{56}$	2.10	2.17
	$C_{15} = -C_{25}$	–0.33	–0.85
	C_{33}	12.83	14.86
	$C_{44} = C_{55}$	4.27	3.19
	C_{66}	6.00	5.34
extrema of Young's modulus / GPa	E_{min}	4.26	4.86
	E_{max}	19.21	16.89
elastic anisotropy[54]	A_L	0.863	0.930
bulk modulus (Reuss average) / GPa	K_R	12.52	14.77
extrema of linear compressibility / TPa^{-1}	β_{min}	–7.7	3.7
	β_{max}	95.2	60.4

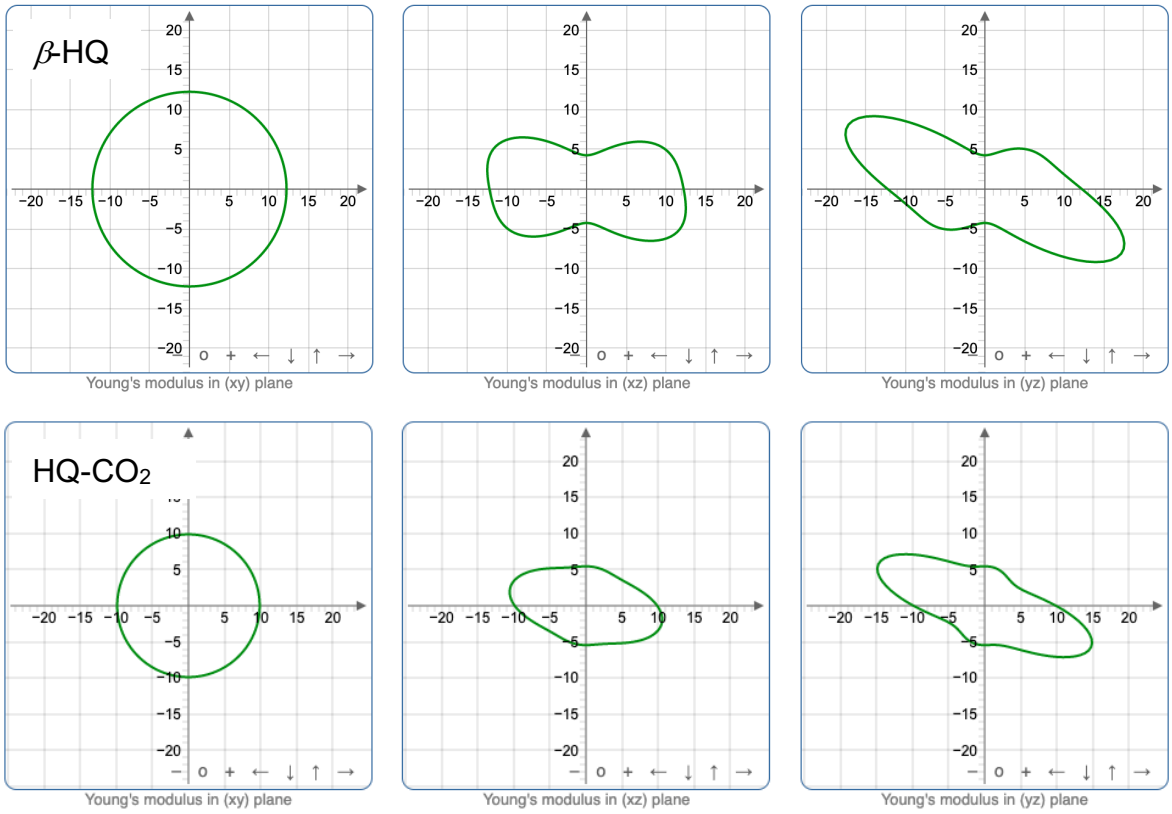

Figure S9. S-HF-3c Young's modulus in three orthogonal planes for β-HQ and HQ-CO_2 (units are GPa). The cartesian axes are defined in terms of the cell axes: $\boldsymbol{z}$ // $\boldsymbol{c}$, $\boldsymbol{y}$ // $\boldsymbol{b}$ and $\boldsymbol{x}$ // $\boldsymbol{z} \times \boldsymbol{y}$.

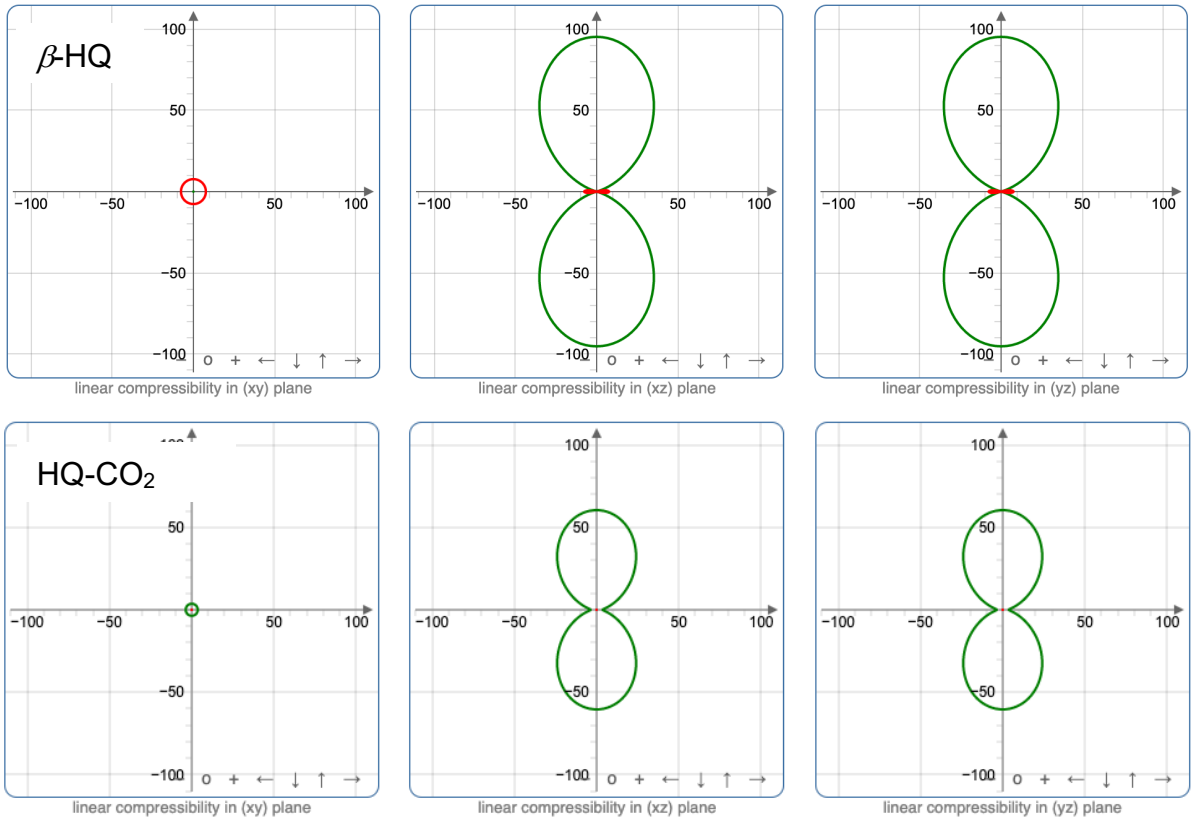

Figure S10. S-HF-3c linear compressibility in three orthogonal planes (units are TPa^{-1}). The cartesian axes are defined in terms of the cell axes: ***z*** // ***c***, ***y*** // ***b*** and ***x*** // ***z*** × ***y***.

S7. Supporting references

(1) Hirotsu, K.; Kamitori, S.; Higuchi, T.; Tabushi, I.; Yamamura, K.; Nonoguchi, H., The structures of macrocyclic heterocyclophane inclusion complexes, *J. Inclusion Phenom.* **1984**, *2*, 215-222.
(2) Miyahara, Y.; Abe, K.; Inazu, T., "Molecular" molecular sieves: Lid-free decamethylcucurbit[5]uril absorbs and desorbs gases selectively, *Angew. Chem., Int. Ed.* **2002**, *41*, 3020-3023.
(3) Clarke, C. S.; Haynes, D. A.; Rawson, J. M.; Bond, A. D., Small molecule fixation by a dithiadiazolyl radical: X-ray crystal structures of (CF3C6H3FCNSSN)2 and (CF3C6H3FCNSSN)2?G (G = N2, Ar, CO2 and SO2), *Chem. Commun.* **2003**, 2774.
(4) Udachin, K. A.; Moudrakovski, I. L.; Enright, G. D.; Ratcliffe, C. I.; Ripmeester, J. A., Loading-dependent structures of CO2 in the flexible molecular van der Waals host p-tert-butylcalix[4]arene with 1 : 1 and 2 : 1 guest-host stoichiometries, *Phys Chem Chem Phys* **2008**, *10*, 4636-4643.
(5) Saint Martin, S.; Marre, S.; Guionneau, P.; Cansell, F.; Renouard, J.; Marchetto, V.; Aymonier, C., Host-Guest Inclusion Compound from Nitramine Crystals Exposed to Condensed Carbon Dioxide, *Chem. Eur. J.* **2010**, *16*, 13473-13478.
(6) Xu, J.; Zheng, S.; Huang, S.; Tian, Y.; Liu, Y.; Zhang, H.; Sun, J., Host-guest energetic materials constructed by incorporating oxidizing gas molecules into an organic lattice cavity toward achieving highly-energetic and low-sensitivity performance, *Chem. Commun.* **2019**, *55*, 909-912.
(7) Zharkov, M. N.; Kuchurov, I. V.; Zlotin, S. G., Micronization of CL-20 using supercritical and liquefied gases, *CrystEngComm* **2020**, *22*, 7549-7555.
(8) Kim, H.; Kim, Y.; Yoon, M.; Linn, S.; Park, S.; Seo, G.; Kim, K., Highly Selective Carbon Dioxide Sorption in an Organic Molecular Porous Material, *J. Am. Chem. Soc.* **2010**, *132*, 12200-12202.
(9) Tsue, H.; Takahashi, H.; Ishibashi, K.; Inoue, R.; Shimizu, S.; Takahashi, D.; Tamura, R., Crystallographic analysis of CO2sorption state in seemingly nonporous molecular crystal of azacalix[4]arene tetramethyl ether exhibiting highly selective CO2uptake, *CrystEngComm* **2012**, *14*, 1021-1026.
(10) He, J.-B.; Ji, Y.-N.; Hu, D.-B.; Zhang, S.; Yan, H.; Liu, X.-C.; Luo, H.-R.; Zhu, H.-J., Structure and absolute configuration of penicilliumine, a new alkaloid from Penicillium commune 366606, *Tet. Lett.* **2014**, *55*, 2684-2686.
(11) Jacobs, T.; Smith, V. J.; Thomas, L. H.; Barbour, L. J., Carbon dioxide entrapment in an organic molecular host, *Chem. Commun.* **2014**, *50*, 85-87.
(12) Baek, S. B.; Moon, D.; Graf, R.; Cho, W. J.; Park, S. W.; Yoon, T. U.; Cho, S. J.; Hwang, I. C.; Bae, Y. S.; Spiess, H. W.; Lee, H. C.; Kim, K. S., High-temperature in situ crystallographic observation of reversible gas sorption in impermeable organic cages, *Proc. Natl. Acad. Sci. U.S.A.* **2015**, *112*, 14156-14161.
(13) Kane, C. M.; Ugono, O.; Barbour, L. J.; Holman, K. T., Many Simple Molecular Cavitands Are Intrinsically Porous (Zero-Dimensional Pore) Materials, *Chem. Mater.* **2015**, *27*, 7337-7354.
(14) Torré, J.-P.; Coupan, R.; Chabod, M.; Pere, E.; Labat, S.; Khoukh, A.; Brown, R. N.; Sotiropoulos, J.-M.; Gornitzka, H., CO2–Hydroquinone Clathrate: Synthesis, Purification, Characterization and Crystal Structure, *Cryst. Growth Des.* **2016**, *16*, 5330-5338.
(15) Kane, C. M.; Banisafar, A.; Dougherty, T. P.; Barbour, L. J.; Holman, K. T., Enclathration and Confinement of Small Gases by the Intrinsically 0D Porous Molecular Solid, Me,H,SiMe2, *J. Am. Chem. Soc.* **2016**, *138*, 4377-4392.
(16) Bassanetti, I.; Bracco, S.; Comotti, A.; Negroni, M.; Bezuidenhout, C.; Canossa, S.; Mazzeo, P. P.; Marchió, L.; Sozzani, P., Flexible porous molecular materials responsive to CO2, CH4 and Xe stimuli, *Journal of Materials Chemistry A* **2018**, *6*, 14231-14239.
(17) Nikolayenko, V. I.; Castell, D. C.; van Heerden, D. P.; Barbour, L. J., Guest-Induced Structural Transformations in a Porous Halogen-Bonded Framework, *Angew. Chem., Int. Ed.* **2018**, *57*, 12086-12091.
(18) Torré, J.-P.; Gornitzka, H.; Coupan, R.; Dicharry, C.; Pérez-Rodríguez, M.; Comesaña, A.; Piñeiro, M. M., Insights into the Crystal Structure and Clathration Selectivity of Organic Clathrates Formed with Hydroquinone and (CO2 + CH4) Gas Mixtures, *The Journal of Physical Chemistry C* **2019**, *123*, 14582-14590.
(19) Niu, L.; Xing, S.; Li, X.; Chen, H., Synthesis of the Fused Tetracyclic Thiazinan-4-one Derivatives and Their Anti-tumor

Activitiy, *Chinese Journal of Organic Chemistry* **2019**, *39*, 771-777.
(20) Rigaku, O. D., CrysAlis Pro (Rigaku Oxford Diffraction Ltd, Yarton, Oxfordshire, UK). 2019.
(21) Dolomanov, O. V.; Bourhis, L. J.; Gildea, R. J.; Howard, J. A. K.; Puschmann, H., OLEX2: a complete structure solution, refinement and analysis program, *J. Appl. Cryst.* **2009**, *42*, 339-341.
(22) (a) Sheldrick, G. M., SHELXT - Integrated space-group and crystal-structure determination, *Acta Crystallogr., Sect. A: Found. Adv.* **2015**, *71*, 3-8. (b) Sheldrick, G. M., Crystal structure refinement with SHELXL, *Acta Crystallogr., Sect. C: Struct. Chem.* **2015**, *71*, 3-8.
(23) Farrugia, L. J., WinGX and ORTEP for Windows: an update, *J. Appl. Crystallogr.* **2012**, *45*, 849-854.
(24) (a) Piltz, R. O., Accurate data processing for neutron Laue diffractometers, *J. Appl. Cryst.* **2018**, *51*, 635-645. (b) Piltz, R. O., LaueG software for displaying and processing neutron Laue images, *J. Appl. Cryst.* **2018**, *51*, 963-965.
(25) Wilkinson, C.; Khamis, H. W.; Stansfield, R. F. D.; McIntyre, G. J., Integration of single-crystal reflections using area multidetectors, *J. Appl. Cryst.* **1988**, *21*, 471-478.
(26) Betteridge, P. W.; Carruthers, J. R.; Cooper, R. I.; Prout, K.; Watkin, D. J., CRYSTALS version 12: software for guided crystal structure analysis, *J. Appl. Cryst.* **2003**, *36*, 1487.
(27) Ilczyszyn, M.; Selent, M.; Ilczyszyn, M. M., Participation of xenon guest in hydrogen bond network of beta-hydroquinone crystal, *J. Phys. Chem. A* **2012**, *116*, 3206-3214.
(28) Eikeland, E.; Thomsen, M. K.; Overgaard, J.; Spackman, M. A.; Iversen, B. B., Intermolecular Interaction Energies in Hydroquinone Clathrates at High Pressure, *Cryst. Growth Des.* **2017**, *17*, 3834-3846.
(29) Palin, D. M.; Powell, H. M., The structure of molecular compounds. Part VI. The b-type clathrate compounds of quinol, *J. Chem. Soc.* **1948**, 815-821.
(30) Peyronel, G.; Barbieri, G., On some new clathrates of hydrquinone, *Journal of Inorganic and Nuclear Chemistry* **1958**, *8*, 582-585.
(31) McAdie, H. G., Thermal decomposition of molecular complexes. IV. Further studies of the b-quinol clathrates, *Can. J. Chem.* **1966**, *44*, 1373-1385.
(32) Lee, J.-W.; Yoon, J.-H., Preferential Occupation of CO2 Molecules in Hydroquinone Clathrates Formed from CO2/N2 Gas Mixtures, *The Journal of Physical Chemistry C* **2011**, *115*, 22647-22651.
(33) Lee, Y. J.; Han, K. W.; Jang, J. S.; Jeon, T. I.; Park, J.; Kawamura, T.; Yamamoto, Y.; Sugahara, T.; Vogt, T.; Lee, J. W.; Lee, Y.; Yoon, J. H., Selective CO2 trapping in guest-free hydroquinone clathrate prepared by gas-phase synthesis, *ChemPhysChem* **2011**, *12*, 1056-1059.
(34) Lee, J.-W.; Dotel, P.; Park, J.; Yoon, J.-H., Separation of CO2 from flue gases using hydroquinone clathrate compounds, *Korean Journal of Chemical Engineering* **2015**, *32*, 2507-2511.
(35) Yoon, S. J.; Lee, D.; Yoon, J.-H.; Lee, J.-W., Swapping and Enhancement of Guest Occupancies in Hydroquinone Clathrates Using CH4 and CO2, *Energy & Fuels* **2019**, *33*, 6634-6640.
(36) Blessing, R. H., On the differences between x-ray and neutron thermal vibration parameters, *Acta Crystallogr., Sect. B: Struct. Sci.* **1995**, *51*, 816-823.
(37) Stewart, R. F. In *Electron and Magnetization Densities in Molecules and Solids*; Becker, P., Ed.; Plenum: New York, 1980, p 427-431.
(38) (a) Dovesi, R.; Saunders, V. R.; Roetti, C.; Orlando, R.; Zicovich-Wilson, C. M.; Pascale, F.; Civalleri, B.; Doll, K.; Harrison, N. M.; Bush, I. J.; D'Arco, P.; Llunell, M.; Causà, M.; Noël, Y.; Maschio, L.; Erba, A.; Rerat, C.; Casassa, S., CRYSTAL17 User's Manual, University of Torino, 2017. (b) Dovesi, R.; Erba, A.; Orlando, R.; Zicovich-Wilson, C. M.; Civalleri, B.; Maschio, L.; Rérat, M.; Casassa, S.; Baima, J.; Salustro, S.; Kirtman, B., Quantum-mechanical condensed matter simulations with CRYSTAL, *WIREs Comput. Mol. Sci.* **2018**, *8*, e1360.
(39) (a) Becke, A. D., Density-functional thermochemistry. III. The role of exact exchange, *J. Chem. Phys.* **1993**, *98*, 5648-5652. (b) Stephens, P. J.; Devlin, F. J.; Chabalowski, C. F.; Frisch, M. J., Ab-initio calculation of vibrational absorption and circular-dichroism spectra using density-functional force-fields, *J. Phys. Chem.* **1994**, *98*, 11623-11627.
(40) Peintinger, M. F.; Oliveira, D. V.; Bredow, T., Consistent gaussian basis sets of triple-zeta valence with polarization quality for solid-state calculations, *J. Comput. Chem.* **2013**, *34*, 451-459.

(41) (a) Kresse, G.; Hafner, J., Abinitio molecular-dynamics for liquid-metals, *Phys. Rev. B* **1993**, *47*, 558-561. (b) Kresse, G.; Hafner, J., Ab-initio molecular-dynamics simulation of the liquid-metal amorphous-semiconductor transition in germanium, *Phys. Rev. B* **1994**, *49*, 14251-14269. (c) Kresse, G.; Furthmuller, J., Efficiency of ab-initio total energy calculations for metals and semiconductors using a plane-wave basis set, *Comput. Mater. Sci.* **1996**, *6*, 15-50. (d) Kresse, G.; Furthmuller, J., Efficient iterative schemes for ab initio total-energy calculations using a plane-wave basis set, *Phys. Rev. B* **1996**, *54*, 11169-11186.
(42) Perdew, J. P.; Burke, K.; Ernzerhof, M., Generalized gradient approximation made simple, *Phys. Rev. Lett.* **1996**, *77*, 3865-3868.
(43) Grimme, S.; Antony, J.; Ehrlich, S.; Krieg, H., A Consistent and Accurate Ab Initio Parametrization of Density Functional Dispersion Correction (DFT-D) for the 94 Elements H-Pu, *J. Chem. Phys.* **2010**, *132*, 154104.
(44) Grimme, S.; Ehrlich, S.; Goerigk, L., Effect of the Damping Function in Dispersion Corrected Density Functional Theory, *J. Comput. Chem.* **2011**, *32*, 1456-1465.
(45) Blochl, P. E., Projector augmented-wave method, *Phys. Rev. B* **1994**, *50*, 17953-17979.
(46) Kresse, G.; Joubert, D., From ultrasoft pseudopotentials to the projector augmented-wave method, *Phys. Rev. B* **1999**, *59*, 1758-1775.
(47) Mackenzie, C. F.; Spackman, P. R.; Jayatilaka, D.; Spackman, M. A., CrystalExplorer model energies and energy frameworks: Extension to metal coordination compounds, organic salts, solvates and open shell systems, *IUCrJ* **2017**, *4*, 575-587.
(48) Frisch, M. J.; Trucks, G. W.; Schlegel, H. B.; Scuseria, G. E.; Robb, M. A.; Cheeseman, J. R.; Scalmani, G.; Barone, V.; Mennucci, B.; Petersson, G. A.; Nakatsuji, H.; Caricato, M.; Li, X.; Hratchian, H. P.; Izmaylov, A. F.; Bloino, J.; Zheng, G.; Sonnenberg, J. L.; Hada, M.; Ehara, M.; Toyota, K.; Fukuda, R.; Hasegawa, J.; Ishida, M.; Nakajima, T.; Honda, Y.; Kitao, O.; Nakai, H.; Vreven, T.; Montgomery Jr., J. A.; Peralta, J. E.; Ogliaro, F. o.; Bearpark, M. J.; Heyd, J.; Brothers, E. N.; Kudin, K. N.; Staroverov, V. N.; Kobayashi, R.; Normand, J.; Raghavachari, K.; Rendell, A. P.; Burant, J. C.; Iyengar, S. S.; Tomasi, J.; Cossi, M.; Rega, N.; Millam, N. J.; Klene, M.; Knox, J. E.; Cross, J. B.; Bakken, V.; Adamo, C.; Jaramillo, J.; Gomperts, R.; Stratmann, R. E.; Yazyev, O.; Austin, A. J.; Cammi, R.; Pomelli, C.; Ochterski, J. W.; Martin, R. L.; Morokuma, K.; Zakrzewski, V. G.; Voth, G. A.; Salvador, P.; Dannenberg, J. J.; Dapprich, S.; Daniels, A. D.; Farkas, Ã. d. n.; Foresman, J. B.; Ortiz, J. V.; Cioslowski, J.; Fox, D. J., Gaussian 09, Revision D.01, Gaussian, Inc., 2009.
(49) Togo, A.; Tanaka, I., First principles phonon calculations in materials science, *Scripta Materialia* **2015**, *108*, 1-5.
(50) Perger, W. F.; Criswell, J.; Civalleri, B.; Dovesi, R., Ab-initio calculation of elastic constants of crystalline systems with the CRYSTAL code, *Comp. Phys. Comm.* **2009**, *180*, 1753-1759.
(51) Cutini, M.; Civalleri, B.; Corno, M.; Orlando, R.; Brandenburg, J. G.; Maschio, L.; Ugliengo, P., Assessment of Different Quantum Mechanical Methods for the Prediction of Structure and Cohesive Energy of Molecular Crystals, *J. Chem. Theory Comput.* **2016**, *12*, 3340-3352.
(52) Thomas, S. P.; Halabi, J. M.; Karothu, D. P.; Spackman, P. R.; Naumov, P.; Spackman, M. A., In preparation, **2020**.
(53) Gaillac, R.; Pullumbi, P.; Coudert, F. X., ELATE: an open-source online application for analysis and visualization of elastic tensors, *J. Phys.: Condens. Matter* **2016**, *28*, 275201.
(54) Kube, C. M., Elastic anisotropy of crystals, *AIP Advances* **2016**, *6*, 095209.